# Chapter 7
# Flow in Binary Media with Heterogeneous Air-Entry Pressure

The upscaled models presented in Chap. 6 are based on the assumption that the Richards equation is a valid model of water flow at the local (Darcy) scale. This, however, is not necessarily the case, especially during transition between unsaturated and water-saturated conditions in porous media showing distinct and locally variable values of the entry pressure. As the continuity of the air phase and its connection to the atmosphere may be lost, the assumptions underlying the Richards model no longer hold, and the description should be based on the full two-phase flow model. This chapter presents the development of an upscaled model which accounts for heterogeneity in the air entry pressure and which is applicable to capillary-dominated flow in media showing moderate permeability contrast. It is shown that, after appropriate modification, the upscaled Richards equation shows a better agreement with the reference two-phase model than the non-upscaled Richards equation solved for explicitly represented heterogeneous structure. The following presentation is based on papers [8, 9].

## 7.1 Upscaled Model of Two-phase Capillary Flow

### *7.1.1 Basic Assumptions*

The porous medium is characterized by the same binary structure as considered in Chap. 6, see Fig. 6.1, i.e. it is composed of a continuous background material, denoted by superscript I and disconnected inclusions, denoted by superscript II. Furthermore, it is assumed that the condition of separation of scales, given by Eq. (6.1), is satisfied. At the local scale, the flow of water and air in each region is described by Eqs. (2.50)–(2.51), with the storage terms written according to Eq. (2.52):

A. Szymkiewicz, *Modelling Water Flow in Unsaturated Porous Media*,
GeoPlanet: Earth and Planetary Sciences, DOI: 10.1007/978-3-642-23559-7_7,

$$\theta_{\mathrm{w}}^{I} c_{\mathrm{w}} \frac{\partial p_{\mathrm{w}}^{I}}{\partial t} + \rho_{\mathrm{w}}^{I} \frac{\partial \theta_{\mathrm{w}}^{I}}{\partial t} - \nabla \left[ \rho_{w}^{I} \frac{\mathsf{k}_{\mathrm{w}}^{I}}{\mu_{\mathrm{w}}} \left( \nabla p_{\mathrm{w}}^{I} - \rho_{\mathrm{w}}^{I} \mathbf{g} \right) \right] = 0 \quad \text{in } \Omega^{I}, \tag{7.1}$$

$$\theta_{\mathrm{a}}^{I} c_{\mathrm{a}} \frac{\partial p_{\mathrm{a}}^{I}}{\partial t} + \rho_{\mathrm{a}}^{I} \frac{\partial \theta_{\mathrm{a}}^{I}}{\partial t} - \nabla \left[ \rho_{a}^{I} \frac{\mathsf{k}_{\mathrm{a}}^{I}}{\mu_{\mathrm{a}}} \left( \nabla p_{\mathrm{a}}^{I} - \rho_{\mathrm{a}}^{I} \mathbf{g} \right) \right] = 0 \quad \text{in } \Omega^{I}, \tag{7.2}$$

$$\theta_{\mathrm{w}}^{II} c_{\mathrm{w}} \frac{\partial p_{\mathrm{w}}^{II}}{\partial t} + \rho_{\mathrm{w}}^{II} \frac{\partial \theta_{\mathrm{w}}^{II}}{\partial t} - \nabla \left[ \rho_{w}^{II} \frac{\mathsf{k}_{\mathrm{w}}^{II}}{\mu_{\mathrm{w}}} \left( \nabla p_{\mathrm{w}}^{II} - \rho_{\mathrm{w}}^{II} \mathbf{g} \right) \right] = 0 \quad \text{in } \Omega^{II}, \tag{7.3}$$

$$\theta_{\mathrm{a}}^{II} c_{\mathrm{a}} \frac{\partial p_{\mathrm{a}}^{II}}{\partial t} + \rho_{\mathrm{a}}^{II} \frac{\partial \theta_{\mathrm{a}}^{II}}{\partial t} - \nabla \left[ \rho_{a}^{II} \frac{\mathsf{k}_{\mathrm{a}}^{II}}{\mu_{\mathrm{a}}} \left( \nabla p_{\mathrm{a}}^{II} - \rho_{\mathrm{a}}^{II} \mathbf{g} \right) \right] = 0 \quad \text{in } \Omega^{II}, \tag{7.4}$$

where $c_{\mathrm{w}}$ and $c_{\mathrm{a}}$ are the compressibility coefficients of water and air. The conditions at the interface $\Gamma$ vary, depending on the saturation of the two materials, as discussed in the following sections. Similarly to the previous chapter, the characteristic time of the process is chosen as the time of flow at the macroscopic scale in the background material. However, in contrast to the previous chapter, the analysis is limited to the case when the permeabilities of the two materials are of the same order of magnitude.

As far as the local balance of driving forces is considered, we assume that at the scale of a single periodic cell the capillary forces dominate over the viscous and gravitational forces. These conditions can be quantified by two dimensionless numbers. The Bond number $\mathscr{R}_{\mathrm{g}}$ represents the ratio of gravitational to capillary forces, while the capillary number $\mathscr{R}_{\mathrm{c}}$ represents the ratio of viscous to capillary forces, e.g. [2]:

$$\mathscr{R}_{\mathrm{g}} = \frac{\left( \rho_{\mathrm{w}}^{(c)} - \rho_{\mathrm{a}}^{(c)} \right) g^{(c)} l_{\mathrm{g}}}{p_{\mathrm{c}}^{(c)}} = \mathscr{O}(\varepsilon) \ll 1, \tag{7.5}$$

$$\mathscr{R}_{\mathrm{c}} = \frac{\mu_{\alpha}^{(c)} v_{\alpha}^{(c)} l_{\mathrm{c}}}{k_{\mathrm{s}}^{(c)} p_{\mathrm{c}}^{(c)}} = \mathscr{O}(\varepsilon) \ll 1, \tag{7.6}$$

where the superscript $(c)$ denotes characteristic values. The characteristic length for the Bond number $l_{\mathrm{g}}$ can be assumed equal to the vertical dimension of a single heterogeneity (inclusion), while the length in the capillary number $l_{\mathrm{c}}$ can be taken as the dimension of the heterogeneity in the direction of the flow. A more detailed discussion of the role of dimensionless numbers in upscaling of two-phase flow can be found in [2, 3, 7].

The form of the upscaled model depends on the continuity of the non-wetting fluid across the material interface $\Gamma$ between the background material and inclusions. One can distinguish three cases, which are described in the following paragraphs.

### 7.1.2 Capillary Flow without Entry Pressure Effects

If both air and water are mobile at either side of the material interface, one can assume that the pressures in each of the phases (and consequently also the capillary pressure) are continuous across the background-inclusion interface:

$$p_{\mathrm{w}}^{I} = p_{\mathrm{w}}^{II} \quad \text{on } \Gamma, \tag{7.7}$$

$$p_{\mathrm{a}}^{I} = p_{\mathrm{a}}^{II} \quad \text{on } \Gamma. \tag{7.8}$$

Moreover, the continuity of normal mass fluxes across the interface can be assumed:

$$-\rho_{\mathrm{w}}^{I}\frac{\mathsf{k}_{\mathrm{w}}^{I}}{\mu_{\mathrm{w}}}\left(\nabla p_{\mathrm{w}}^{I}-\rho_{\mathrm{w}}^{I}\,\mathbf{g}\right)\mathbf{n}_{\Gamma} = -\rho_{\mathrm{w}}^{II}\frac{\mathsf{k}_{\mathrm{w}}^{II}}{\mu_{\mathrm{w}}}\left(\nabla p_{\mathrm{w}}^{II}-\rho_{\mathrm{w}}^{II}\,\mathbf{g}\right)\mathbf{n}_{\Gamma} \quad \text{on } \Gamma, \tag{7.9}$$

$$-\rho_{\mathrm{a}}^{I}\frac{\mathsf{k}_{\mathrm{a}}^{I}}{\mu_{\mathrm{a}}}\left(\nabla p_{a}^{I}-\rho_{\mathrm{a}}^{I}\,\mathbf{g}\right)\mathbf{n}_{\Gamma} = -\rho_{\mathrm{a}}^{II}\frac{\mathsf{k}_{\mathrm{a}}^{II}}{\mu_{\mathrm{a}}}\left(\nabla p_{\mathrm{a}}^{II}-\rho_{\mathrm{a}}^{II}\,\mathbf{g}\right)\mathbf{n}_{\Gamma} \quad \text{on } \Gamma. \tag{7.10}$$

where $\mathbf{n}_{\Gamma}$ is the unit vector normal to the interface $\Gamma$.

For the above interface conditions, Saez et al. [6] derived a homogenized model of the following form:

$$\theta_{\mathrm{w}}^{\mathrm{eff}}\,c_{\mathrm{w}}\frac{\partial p_{\mathrm{w}}^{\mathrm{eff}}}{\partial t}+\rho_{\mathrm{w}}^{\mathrm{eff}}\frac{\partial \theta_{\mathrm{w}}^{\mathrm{eff}}}{\partial t}-\nabla\left[\rho_{\mathrm{w}}^{\mathrm{eff}}\frac{\mathsf{k}_{\mathrm{w}}^{\mathrm{eff}}}{\mu_{\mathrm{w}}}\left(\nabla p_{\mathrm{w}}^{\mathrm{eff}}-\rho_{\mathrm{w}}^{\mathrm{eff}}\,\mathbf{g}\right)\right]=0, \tag{7.11}$$

$$\theta_{\mathrm{a}}^{\mathrm{eff}}\,c_{\mathrm{a}}\frac{\partial p_{\mathrm{a}}^{\mathrm{eff}}}{\partial t}+\rho_{\mathrm{a}}^{\mathrm{eff}}\frac{\partial \theta_{\mathrm{a}}^{\mathrm{eff}}}{\partial t}-\nabla\left[\rho_{\mathrm{a}}^{\mathrm{eff}}\frac{\mathsf{k}_{\mathrm{a}}^{\mathrm{eff}}}{\mu_{\mathrm{a}}}\left(\nabla p_{\mathrm{a}}^{\mathrm{eff}}-\rho_{\mathrm{a}}^{\mathrm{eff}}\,\mathbf{g}\right)\right]=0. \tag{7.12}$$

This model can be regarded as a two-phase counterpart of the upscaled Richards equation with local equilibrium, described in Sect. 6.3.1. The pressures in each fluid phase is uniform within a unit cell at the zeroth order of approximation. Consequently, the phase densities are also uniform, their values corresponding to the phase pressures, $\rho_{\alpha}^{\mathrm{eff}}=\rho_{\alpha}\left(p_{\mathrm{c}}^{\mathrm{eff}}\right)$. Moreover, the capillary pressure:

$$p_{\mathrm{c}}^{\mathrm{eff}}=p_{\mathrm{a}}^{\mathrm{eff}}-p_{\mathrm{w}}^{\mathrm{eff}}$$

is uniform in a periodic cell, i.e. local capillary equilibrium conditions occur. However, the saturations and phase contents are different in each of the two regions, because the background material and inclusions are characterized by different $p_{\mathrm{c}}-S_{\mathrm{ew}}$ curves. The effective (average) porosity and volumetric phase contents are defined similarly as in the case of the upscaled Richards equation:

$$\phi^{\mathrm{eff}}=w^{I}\,\phi^{I}+w^{II}\phi^{II}, \tag{7.13}$$

$$\theta_{\alpha}^{\mathrm{eff}}=w^{I}\,\theta_{\alpha}^{I}\left(p_{\mathrm{c}}^{\mathrm{eff}}\right)+w^{II}\theta_{\alpha}^{II}\left(p_{\mathrm{c}}^{\mathrm{eff}}\right), \tag{7.14}$$

$$S_{\alpha}^{\mathrm{eff}}=\theta_{\alpha}^{\mathrm{eff}}/\phi^{\mathrm{eff}}. \tag{7.15}$$

In order to simplify the presentation, it is assumed that the residual saturations of air and water are zero in each material, i.e. the saturations can change in the whole range of values between 0 and 1:

$$0 \leq S_\alpha^\iota \leq 1, \tag{7.16}$$

$$0 \leq \theta_\alpha^\iota \leq \phi, \tag{7.17}$$

where $\iota = 1, 2$ is the index of porous material. This assumption does not reduce the generality of the model and the case with non-zero residual saturations is described in [8].

The effective permeability tensors for each phase depend on the effective capillary pressure. They are defined in a similar way as the effective water permeability in the case of upscaled Richards equation, Eqs. (6.43)–(6.47). For the chosen value of the effective capillary pressure, a corresponding piecewise-constant distribution of the phase permeability is assumed, with $\mathsf{k}_\alpha^I\left(p_\mathrm{c}^\mathrm{eff}\right)$ in the background material and $\mathsf{k}_\alpha^{II}\left(p_\mathrm{c}^\mathrm{eff}\right)$ in the inclusions. Next, the local boundary value problem, Eqs. (6.43)–(6.46), is solved for each spatial direction $m$ to obtain the corresponding auxiliary variable $\chi_m$, which has to satisfy periodic boundary conditions. Based on these results, the entries of the effective tensor are computed from Eq. (6.47). The same procedure applies to water and air phases. Note that the formulation of the local boundary value problem implies that the local permeability values are larger than zero in inclusions as well as in the background material, i.e. the fluid is mobile everywhere in the periodic cell. This is consistent with the assumed conditions at the interface $\Gamma$, Eqs. (7.7)–(7.10). If both materials are isotropic, instead of the solution of the elliptic boundary value problem, simplified approaches can be used to compute the components of the effective tensor for the given pair of scalar values $k_\alpha^I\left(p_\mathrm{c}^\mathrm{eff}\right)$ and $k_\alpha^{II}\left(p_\mathrm{c}^\mathrm{eff}\right)$. However, the procedure outlined above seems more accurate for complex geometries [1, 2].

### *7.1.3 Infiltration with Entry Pressure Effects*

The model described above is valid on condition that both fluid phases are present and mobile on both sides of the interface. If the capillary functions in both inclusions and background do not show air entry pressure (as is the case, for instance, with the van Genuchten model), the air phase disappears from the system for the same value of $p_\mathrm{c} = 0$ in both materials. However, if the capillary functions have distinct entry pressures, which are different in each material, one of the materials becomes fully saturated at a value of the capillary pressure for which the other material remains unsaturated. In such a case an extended capillary pressure continuity condition must be used at the interface $\Gamma$, as discussed in Sect. 2.3.3. The effect of this change on the upscaled model depends on whether the flow is of infiltration or drainage type and whether the entry pressure is higher in the background or in inclusions. This

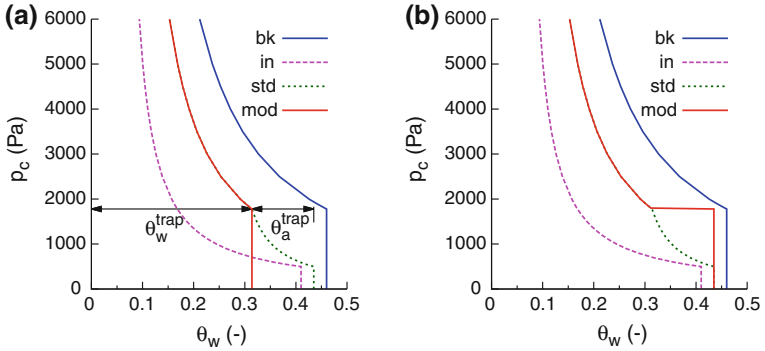


**Fig. 7.1** Upscaled capillary functions for heterogeneous medium with coarse-textured inclusions: **a** infiltration, **b** drainage, (*bk*) background material, (*in*) inclusions, (*std*) standard upscaling method, (*mod*) modified upscaling method accounting for the air entry pressure effects

problem was analyzed for flow in one-dimensional layered medium by [4, 10] and for a multidimensional medium with inclusions by [8].

First, infiltration in a medium with higher entry pressure in the background is considered, $p_e^I > p_e^{II}$. Since the entry pressure is in general inversely proportional to the characteristic size of the pores, the inclusions can be regarded as having coarser texture (larger pores) compared to the finer background material. Initially the medium is dry, which corresponds to a large value of the capillary pressure. As the water infiltrates, the capillary pressure decreases and the saturation in both materials increases. When the value of the entry pressure of the background $p_e^I$ is reached, this material becomes fully saturated with water. However, the water content in inclusions is still below its maximum value, due to the differences in shape of the capillary functions. This is shown schematically in Fig. 7.1a. If capillary equilibrium conditions hold at the Darcy scale, the inclusion becomes surrounded with fully water saturated fine material and the connectivity of the air phase is lost. In contrast, the water phase remains connected throughout the medium, and the continuity of its pressure and normal flux can be assumed at the material interfaces. The difference between the air pressure in inclusions and the pressure in the water phase does not exceed the entry value for the background material, so the air remains trapped in inclusions. The threshold value of the effective water content, which corresponds to the effective capillary pressure equal to the entry pressure of the background, can be written as:

$$\theta_w^{trap} = w^I \phi^I + w^{II} \phi^{II} S_w^{II}\left(p_e^I\right) < \phi^{eff} \tag{7.18}$$

and the corresponding effective water saturation is:

$$S_w^{trap} = \theta_w^{trap}/\phi^{eff} < 1. \tag{7.19}$$

The corresponding values for the air phase:

$$\theta_{\mathrm{a}}^{\mathrm{trap}} = \phi^{\mathrm{eff}} - \theta_{\mathrm{w}}^{\mathrm{trap}}, \tag{7.20}$$

$$S_{\mathrm{a}}^{\mathrm{trap}} = 1 - S_{\mathrm{w}}^{\mathrm{trap}}, \tag{7.21}$$

can be considered as the field-scale residual air content and saturation, respectively. Note that these residual values result only from the presence of material heterogeneities, since the pore-scale residual saturations are neglected here. The actual value of the field-scale residual air content depends on the shapes of the capillary functions of the porous materials, as shown in Fig. 7.1a.

Even if the water pressure increases further, the air phase cannot leave the inclusions. This is in contrast to the model described in the previous section, where further decrease of the capillary pressure results in the corresponding decrease of $\theta_{\mathrm{a}}^{II}$ and $\theta_{\mathrm{a}}^{\mathrm{eff}}$ and the increase of the wetting phase permeability, computed from the solution of the cell problem. Such approach does not take into account the fact that the non-wetting phase cannot leave the inclusions, because it cannot overcome the entry pressure in the background material. In order to include this effect, the interface conditions (7.7)–(7.10) and the upscaled equations should be modified.

In the simplified case of incompressible flow ($c_{\mathrm{w}} = c_{\mathrm{a}} = 0$) the interface conditions can be specified as follows:

$$p_{\mathrm{w}}^{I} = p_{\mathrm{w}}^{II} \quad \text{on } \Gamma, \tag{7.22}$$

$$p_{\mathrm{c}}^{II} = p_{\mathrm{e}}^{I} \quad \text{on } \Gamma, \tag{7.23}$$

where $p_{\mathrm{e}}^{I}$ is the entry pressure of the background material, while for the normal fluxes the following condition holds:

$$-\frac{\mathsf{k}_{\mathrm{w}}^{I}}{\mu_{\mathrm{w}}}\left(\nabla p_{\mathrm{w}}^{I} - \rho_{\mathrm{w}}^{I}\,\mathbf{g}\right)\mathbf{n}_{\Gamma} = -\frac{\mathsf{k}_{\mathrm{w}}^{II}}{\mu_{\mathrm{w}}}\left(\nabla p_{\mathrm{w}}^{II} - \rho_{\mathrm{w}}^{II}\,\mathbf{g}\right)\mathbf{n}_{\Gamma} \quad \text{on } \Gamma, \tag{7.24}$$

$$-\frac{\mathsf{k}_{\mathrm{a}}^{II}}{\mu_{a}}\nabla\left(p_{\mathrm{a}}^{II} - \rho_{\mathrm{a}}^{II}\,\mathbf{g}\right)\mathbf{n}_{\Gamma} = 0 \quad \text{on } \Gamma. \tag{7.25}$$

Note that the air phase pressure is undefined in the background material. With these boundary conditions, the upscaled equation for water becomes:

$$-\nabla\left(\rho_{\mathrm{w}}^{\mathrm{eff}}\,\frac{\mathsf{k}_{\mathrm{w}}^{\mathrm{trap}}}{\mu_{\mathrm{w}}}\left(\nabla p_{\mathrm{w}}^{\mathrm{eff}} - \rho_{\mathrm{w}}^{\mathrm{eff}}\,\mathbf{g}\right)\right) = 0, \tag{7.26}$$

where $\mathsf{k}_{\mathrm{w}}^{\mathrm{trap}}$ is the effective wetting phase permeability obtained from the solution of the local boundary value problem with the relative permeability $k_{\mathrm{rw}}^{I} = 1$ in the background material and $k_{\mathrm{rw}}^{II} = k_{\mathrm{rw}}^{II}\left(p_{\mathrm{e}}^{I}\right)$ in the inclusions. Equation (7.26) describes steady flow, because the water saturation cannot increase any further and the fluids are incompressible. Since the background becomes impermeable with respect to the

non-wetting phase, the corresponding effective permeability becomes $\mathsf{k}_{\mathrm{a}}^{\mathrm{eff}} = 0$. Note that this result cannot be obtained from the solution of the cell problem, because the problem becomes ill-posed when the permeability in any part of the cell is equal to zero. The air content in inclusions is constant:

$$\theta_{\mathrm{a}}^{\mathrm{eff}} = \theta_{\mathrm{a}}^{\mathrm{trap}} = const. \tag{7.27}$$

The capillary pressure in inclusions remains constant and equal to the entry pressure in the background material. Thus, any increase in the water pressure will cause the same increase of the air pressure and the air saturation in inclusions will remain constant. In reality, air can dissolve in water or move upwards in form of small bubbles, but these long-term processes are not accounted for by the present model, based on two-phase immiscible formulation.

If the compressibility of the fluids is taken into account, the model becomes more complex, since the air saturation in inclusions can change due to the compressibility. The relevant upscaled equations can be written as:

$$\theta_{\mathrm{w}}^{\mathrm{eff}}\, c_{\mathrm{w}} \frac{\partial p_{\mathrm{w}}^{\mathrm{eff}}}{\partial t} + \rho_{\mathrm{w}}^{\mathrm{eff}} \frac{\partial \theta_{\mathrm{w}}^{\mathrm{eff}}}{\partial t} - \nabla \left[ \rho_{\mathrm{w}}^{\mathrm{eff}} \frac{\mathsf{k}_{\mathrm{w}}^{\mathrm{trap}}}{\mu_{\mathrm{w}}} \left( \nabla p_{\mathrm{w}}^{\mathrm{eff}} - \rho_{\mathrm{w}}^{\mathrm{eff}} \mathbf{g} \right) \right] = 0, \tag{7.28}$$

$$\theta_{\mathrm{a}}^{II}\, c_{\mathrm{a}} \left( \frac{\partial p_{\mathrm{w}}^{\mathrm{eff}}}{\partial t} + \frac{\partial p_{\mathrm{c}}^{II}}{\partial t} \right) + \rho_{\mathrm{a}}^{II} \frac{\partial \theta_{\mathrm{a}}^{II}}{\partial t} = 0. \tag{7.29}$$

Equation (7.29) states that the mass of the air phase trapped in inclusions should remain constant. Note that the local capillary function is used instead of an upscaled one. The change in saturation is driven by the change in the macroscopic wetting phase pressure. A positive change in $p_{\mathrm{w}}^{\mathrm{eff}}$ causes an increase of the non-wetting phase pressure in inclusions and consequently an increase in the density of the non-wetting fluid. In order to keep the mass constant, the increase in density should be balanced by a decrease of volume occupied by the fluid, which means in turn that the capillary pressure decreases. On the other hand, if $p_{\mathrm{w}}^{\mathrm{eff}}$ decreases, the capillary pressure in inclusions is expected to increase. It can even reach values higher than the entry pressure in the background, which enables the non-wetting fluid to move from inclusions to the background. In this case one should switch again to the model with two continuous phases, described in the previous section. Note also that the saturation change in inclusions due to the compressibility is assumed to be small and its influence on the effective permeability tensor for the water phase is neglected.

### *7.1.4 Drainage with Entry Pressure Effects*

As the second case, drainage in a medium with disconnected coarse inclusions is analyzed. The medium is initially fully saturated with the wetting phase ($S_{\mathrm{w}} = 1$) and starts to be invaded by the non-wetting phase. However, the drainage is possible

only after the critical capillary pressure $p_e^I$ is reached. In the range of capillary pressures below that value, the upscaled equations have the following form:

$$\theta_w^{\text{eff}} c_w \frac{\partial p_w^{\text{eff}}}{\partial t} - \nabla \left[ \rho_w \frac{\mathbf{k}_s^{\text{eff}}}{\mu_w} \left( \nabla p_w^{\text{eff}} - \rho_w^{\text{eff}} \mathbf{g} \right) \right] = 0, \tag{7.30}$$

$$\theta_a^{\text{eff}} = 0 = const, \tag{7.31}$$

where the effective permeability of the wetting phase is equal to the effective intrinsic permeability of the medium.

Initially, there is no capillary equilibrium between inclusions and background, because the capillary pressure in each material is equal to its entry pressure. Once the entry pressure for the matrix is exceeded, the non-wetting phase from the injection zone starts invading the system. As soon as there is a connected path of the non-wetting phase between the injection zone and inclusions, the capillary pressure in inclusions increases, until it equilibrates with the surrounding background material, with the corresponding non-wetting phase saturation in inclusions much larger than the one in the background. This can be represented by a discontinuity in the effective capillary curve, Fig. 7.1b. The water content is constant and equal to the porosity for $p_c^{\text{eff}} < p_e^I$. If the capillary pressure increases by a very small value above the entry pressure of the background, the average water content within a unit cell decreases rapidly to the value corresponding to the capillary equilibrium conditions, because the inclusions desaturate quickly. Such behavior is confirmed by physical experiments on heterogeneous media with disconnected coarse-textured inclusions [11].

Comparing this result with the one obtained for infiltration, one can note that the presence of disconnected coarse inclusions causes a hysteretic behaviour of the heterogeneous medium in the range of capillary pressures below the entry pressure of the background material $p_e^I$. The upscaled capillary and permeability functions are different for infiltration and drainage, as shown in Fig. 7.1a, b. In contrast, application of the standard upscaling procedure based on the assumption of local capillary equilibrium for the whole range of pressures leads to a unique capillary curve for both infiltration and drainage, shown by dotted lines in Fig. 7.1. In the range of capillary pressures above the entry pressure of the background material, all three curves are the same.

The hysteresis results from the presence of material heterogeneities at the Darcy scale and occurs even if locally each of the materials is characterized by a unique capillary curve for infiltration and drainage. The presented approach can be also used when each of the material exhibits hysteresis in its local scale capillary curve. In this case, the method of computing the effective parameters remains the same, but different local scale functions should be used as input, depending on the process which is to be simulated.

The numerical implementation of the upscaled model with entry pressure effects depends on the formulation used in the numerical code to solve the effective equations. As mentioned in Chap. 3, two approaches are possible, i.e. either the principal variables are the pressures of the two fluids and the phase content and permeabilities

are calculated as functions of the pressure difference (capillary pressure) or the principal variables are one of the pressures and one of the saturations and the capillary pressure and permeabilities are calculated as the functions of the saturation. In the first case, one should remember that when the capillary pressure is below the critical value $p_c^{\text{eff}} < p_e^I$, Eqs. (7.14)–(7.15) are no longer valid because the air phase content is either constant or changes very slightly due to the compressibility. In the second case, one should remember that during infiltration the value of the wetting phase content cannot exceed the critical value $\theta_w^{\text{trap}} = \phi^{\text{eff}} - \theta_a^{\text{trap}}$. During the drainage one has to deal with a discontinuous capillary function. For the purposes of consistent numerical solution, it can be replaced by a continuous capillary curve, with linear variation of $\theta_{\text{w}}^{\text{eff}}$ between $p_c^{\text{eff}}$ and $p_c^{\text{eff}} + \upsilon$, where $\upsilon$ is a small number (similar technique for the unsaturated flow equation was used by [11].

Finally, one has to consider an inverse heterogeneity pattern, i.e. fine-textured inclusions with high entry pressure embedded in a continuous coarser background with low entry pressure. During infiltration in such a medium the air phase disappears in inclusions earlier than in the background. Consequently, there is no trapping effect and the standard upscaling procedure can be used for the effective capillary and water permeability functions. In the range of capillary pressures below the entry pressure $p_e^{II}$, the inclusions are impermeable to air, and the cell problem used to define the effective air permeability must be modified. The auxiliary variable $\chi$ is defined only in the background material, while the material interface is considered impermeable. The resulting formulation would be the same as the cell problem describing water permeability in a medium with weakly permeable inclusions, described in Sect. 6.3.2.

The same observation regarding the air permeability holds for drainage. Since the medium starts to drain as soon as the entry pressure of the coarse material is exceeded, there is no discontinuity in the resulting capillary curve. Until the value of the entry pressure for inclusions is reached, the saturation in inclusions remains equal to one, but the effective water content decreases, due to the drainage of the continuous coarse-textured background. In this range the inclusions must be considered as impermeable to air. If the difference in the shape of the capillary curves of the two materials is very large, for high values of the capillary pressure a phenomenon of water phase trapping in fine inclusions may occur, as pointed out by [5]. Since the coarse background is virtually impermeable for water in the range of capillary pressures around the entry pressure of the inclusions, the changes of the capillary pressure in the background (e.g. due to evaporation) are not reflected by the changes of the water saturation in inclusions, because mobile water phase cannot enter the coarse material. Analysis of such phenomena would require accounting for evaporation and vapor transfer and is beyond the scope of this work.

### *7.1.5 Modified Richards Equation*

The above analysis has important implications for the Richards equation. The latter approach differs from the full two-phase model in two important aspects. First,

the volume of water entering or leaving a porous domain is not balanced with the corresponding volume of air which must be displaced by water or replace water, respectively. Second, the water content (or saturation) and permeability are defined as functions of the water pressure, which is assumed to be equal to the negative of the capillary pressure. Thus, it is not possible to describe the air entry effects discussed above using the Richards equation as the model of flow at the Darcy scale.

Consider, for instance, horizontal two-dimensional incompressible flow in a domain containing a single centrally placed inclusion, with entry pressure lower than at the background. Initially, the capillary pressure is equal to the entry pressure in the background material, and the air is at atmospheric pressure ($p_a = 0$). If the water pressure is uniformly increased along the boundaries of the cell, the water pressure in the interior will equilibrate with the new value, due to the continuity of the water phase. According to the two-phase flow model, the pressure of the air in the inclusion will increase by the same value, while the capillary pressure and saturation will remain the same, because the air cannot leave the inclusion through the fully water-saturated background material. However, in the Richards equation the new capillary pressure, taken as the negative of the water pressure, will be smaller than the entry pressure in the background and the corresponding water saturation in the inclusions will increase. Since the increase in water saturation is not balanced with a decrease in air saturation, the result will be such that some amount of water enters the inclusion. If the boundary water pressure is increased to $p_w = 0$, the whole domain will eventually become fully water-saturated.

Differences between the Richards model and the two-phase model are also apparent for drainage of initially fully water-saturated medium with coarse inclusions. Since in the Richards approach the capillary pressure, and consequently the water saturation, depends uniquely on the water pressure, as soon as the water pressure becomes smaller than $(-p_e^{II})$, i.e. the negative of the entry pressure in inclusions, the saturation in inclusions decreases. According to the two-phase model, the drainage cannot start until $p_w$ falls below $(-p_e^{I})$ which is the negative of the entry pressure for the fine-textured background.

In order to overcome this deficiency of the Richards equation, a different approach can be adopted. In this approach, the Richards equation is used not as a Darcy-scale model, but as an upscaled model, with the effective capillary and permeability functions which account for the entry pressure effects in the same way as it was presented for the full two-phase model in the preceding sections. Such a model does not result from a direct upscaling of the Darcy-scale Richards equation. Rather, it should be regarded as a simplification of the two-phase model which is introduced only at the field scale, after the entry pressure effects have been taken into account.

## 7.2 Numerical simulations

In order to illustrate the application of the modified Richards equation, two numerical examples are presented. They concern two-dimensional flow in a heterogeneous medium with inclusions characterized by lower air-entry pressure than the

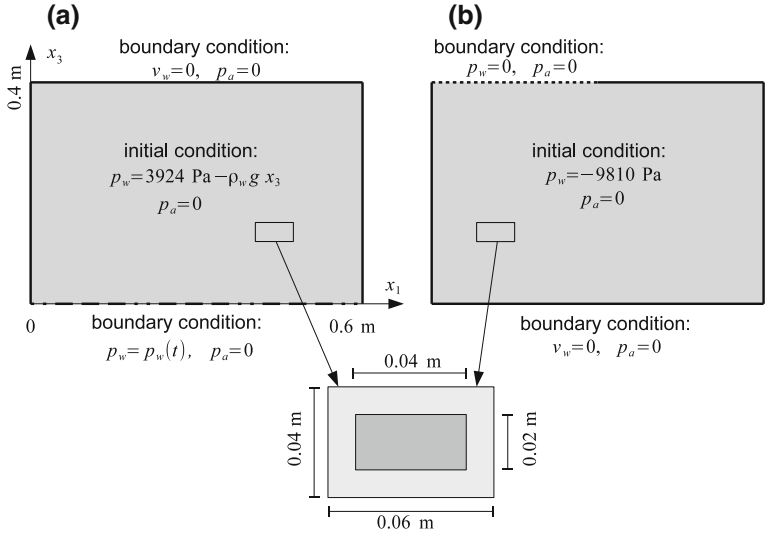


**Fig. 7.2** Geometry and boundary conditions used in the numerical example: **a** water table fluctuation, **b** infiltration in a dry soil

background. For each example, several numerical simulations are provided, based on different models. First, the two-phase model and the Richards equation are solved for the homogeneous background material without inclusions, in order to evaluated the differences between these two approaches due to factors other than material heterogeneity. These solutions are denoted as 2PH-BK and RE-BK, respectively. Next, Darcy-scale solutions are provided for a heterogeneous medium containing inclusions, again using both the two-phase model and the Richards equation. They are denoted as 2PH-DAR and RE-DAR, respectively. Finally, two forms of upscaled Richards equation are solved. The first one is based on the standard approach, which assumes the continuity of the capillary pressure in the periodic cell in the whole range of its values, with the effective parameters defined as in Sect. 7.1.2. This solution is denoted as RE-UPS-1. The second upscaled solution takes into account the air-entry pressure effects, which lead to air trapping during infiltration and retardation of drainage in inclusions, as described in Sects. 7.1.3 and 7.1.4. This solution is referred to as RE-UPS-2.

### *7.2.1 Geometry and Material Parameters*

In each of the two examples, the flow takes place in the same two-dimensional domain represented by a rectangle of 60 by 40 cm, Fig. 7.2. The heterogeneous domain contains 100 inclusions of the dimensions 4 by 2 cm arranged in a regular pattern in the

**Table 7.1** Hydraulic parameters of porous media used in numerical examples

| | $\phi$ (–) | $S_{rw}$ (–) | $S_{ra}$ (–) | $p_e$ (Pa) | $n_b$ (–) | $k_s$ (m$^2$) |
|---|---|---|---|---|---|---|
| Background | 0.4 | 0.0 | 0.0 | 1,200 | 1.5 | 1e−11 |
| Inclusions | 0.4 | 0.0 | 0.0 | 400 | 2.5 | 1e−10 |

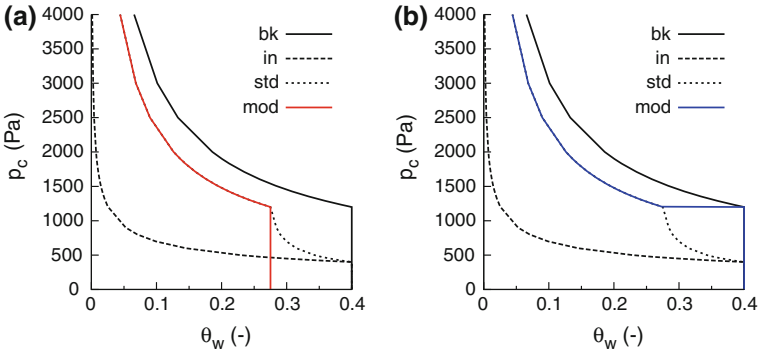


**Fig. 7.3** Capillary functions used in the numerical examples: **a** infiltration, **b** drainage, (*bk*) background material, (*in*) inclusions, (*std*) standard upscaling method, (*mod*) modified upscaling method accounting for the air entry pressure effects

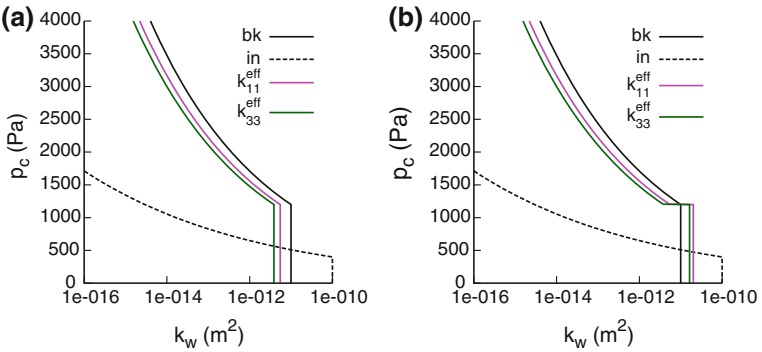


**Fig. 7.4** Water permeability functions used in the numerical examples: **a** infiltration, **b** drainage, (*bk*) background material, (*in*) inclusions. The effective permeability in *horizontal* and *vertical* direction is shown only for the modified method

background material, so that the scale parameter $\varepsilon = 0.1$ for both horizontal and vertical direction. The two porous materials are characterized by Brooks–Corey–Burdine hydraulic functions. Their parameters are listed in Table 7.1. The capillary functions and the relative permeability functions for the wetting phase are shown in Figs. 7.3 and 7.4. Both materials are characterized by a sharp decrease of the water saturation above the air-entry pressure, which is typical for uniformly sized pores.

### 7.2.2 Example 1: Fluctuating Water Table

The considered flow process consists of two stages. At the beginning of the simulation, the domain is fully saturated with water and the position of the water table corresponds to the top of the domain, Fig. 7.2a. The water pressure is distributed hydrostatically from $p_w = 0$ at the top to $p_w = 3924\,\text{Pa}$ at the bottom. In the first phase the water table is gradually lowered until it reaches the bottom of the domain. This is represented by a linear decrease of the water pressure from the initial value at $t = 0$ to the value $p_w = 0$ at $t = 1200\,\text{s}$. The latter value of the pressure is kept constant at the bottom until $t = 7200\,\text{s}$, allowing the water to drain from the domain under the action of the gravity force. Next, the upward infiltration stage begins. The water table is gradually risen to its initial position. Accordingly, the pressure at the bottom increases linearly from $p_w = 0$ at $t = 7200\,\text{s}$ to $p_w = 3924\,\text{Pa}$ at $t = 8400\,\text{s}$. This value remains constant till the end of the simulation at $t = 9600\,\text{s}$. The top of the domain and the vertical edges are considered impermeable for water. For the air flow equation, the initial condition is $p_a = 0$ in the whole domain and a constant boundary value $p_a = 0$ is also imposed at all external boundaries, which represents unobstructed contact with atmospheric air.

The Darcy-scale numerical simulations for heterogeneous domain were performed on a uniform rectangular grid consisting of 60 (horizontal) by 40 (vertical) elements. For the assumed set of boundary conditions the upscaled problems become essentially one-dimensional in the vertical direction, and were solved as such, using 40 elements along $x_3$ axis. The same approach was applied to solve the flow equations in a homogeneous medium (without inclusions).

The results obtained with different models are compared in terms of the average water saturation of the domain, which changes in function of time, as shown in Figs. 7.5 and 7.6. The average water saturation is obtained by dividing the total volume of water in the domain by the total volume of the pores. The drainage and infiltration phases can be easily distinguished as they correspond to the decrease and increase in the average saturation, respectively. In the solutions for homogeneous material, Fig. 7.5, the average water saturation at the end of the drainage–infiltration sequence becomes equal to the initial saturation, i.e. $S_w = 1$. There are virtually no differences between the two-phase model and the Richards equation. In contrast, the presence of inclusions gives rise to significant discrepancies in the results obtained with these two models. In RE-DAR solution the drainage starts earlier than in the 2PH-DAR solution and the amount of drained water is larger, which corresponds to smaller saturation in the domain at the end of drainage phase. The Richards equation does not take into account the fact that drainage of inclusions is only possible if the air is able to reach them, i.e. if the air-entry pressure in the background material is exceeded. The evolution of the average saturation shown in Fig. 7.5 is consistent with the distribution of the local saturation in the domain at $t = 960\,\text{s}$, $t = 7200\,\text{s}$ and $t = 8160\,\text{s}$ shown in Figs. 7.7, 7.8 and 7.9, respectively. It can be seen that according to the Richards equation some inclusions become drained even though the background material around them remains fully saturated. In the 2PH-DAR model, the entry

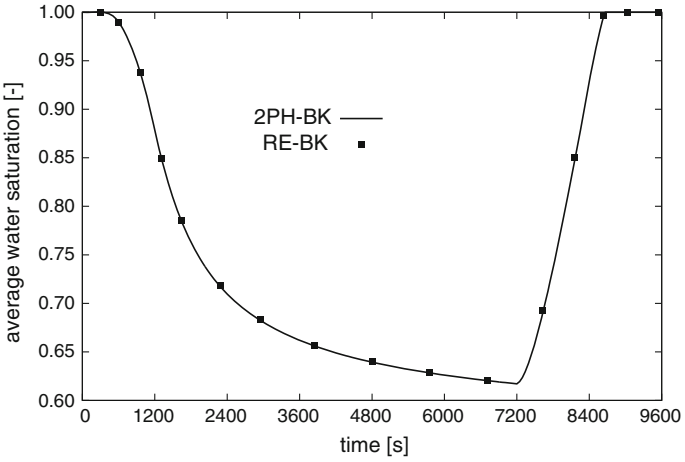


**Fig. 7.5** Example 1: Evolution of the average water saturation in homogeneous background material without inclusions according to the two-phase solution (2PH-BK) and the Richards model (RE-BK)

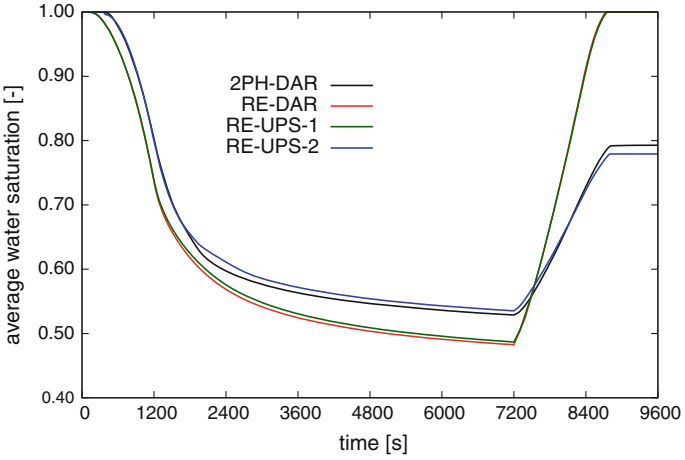


**Fig. 7.6** Example 1: Evolution of the average water saturation in heterogeneous domain according to Darcy-scale two-phase solution (2PH-DAR), Darcy-scale Richards model (RE-DAR), Richards model upscaled in the standard way (RE-UPS-1) and the modified upscaled Richards model (RE-UPS-2)

pressure effects are correctly taken into account and the inclusions remain fully saturated in the lower part of the domain, where the difference between the air pressure and the water pressure does exceed the air entry pressure of the background material.

In the second phase of the flow, which corresponds to upward infiltration, the differences between the two-phase model and the Richards equation become even more

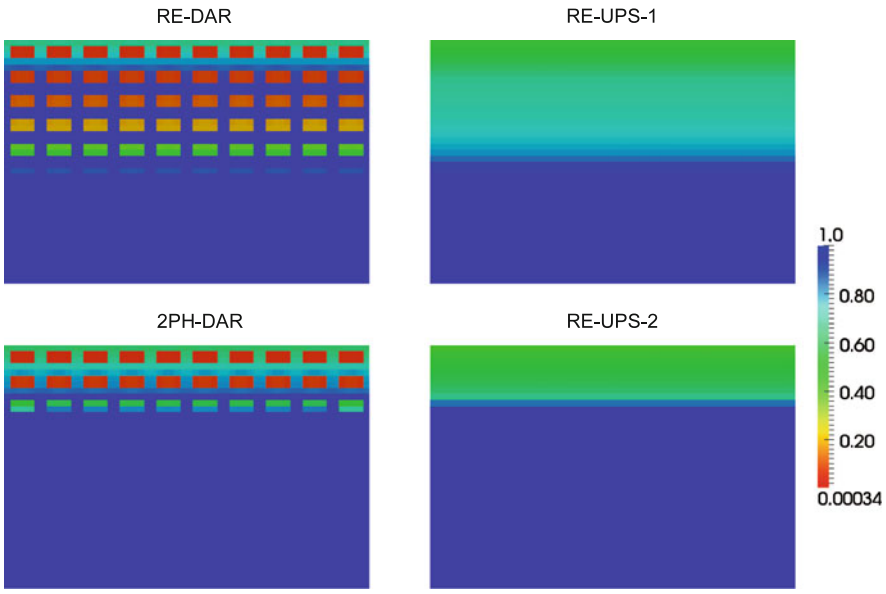


**Fig. 7.7** Example 1: Distribution of the water saturation at $t = 960\,\mathrm{s}$, notation as in Fig. 7.6

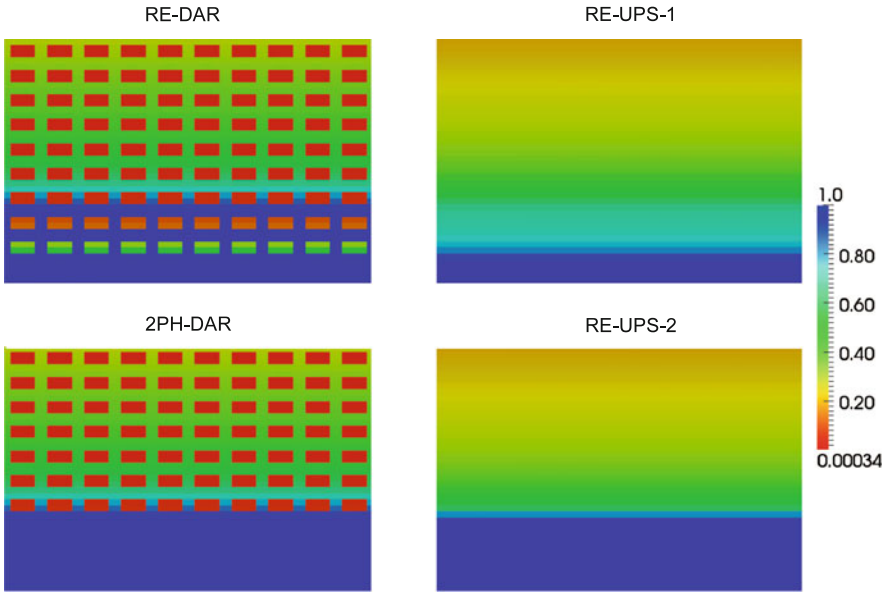


**Fig. 7.8** Example 1: Distribution of the water saturation at $t = 7200\,\mathrm{s}$, notation as in Fig. 7.6

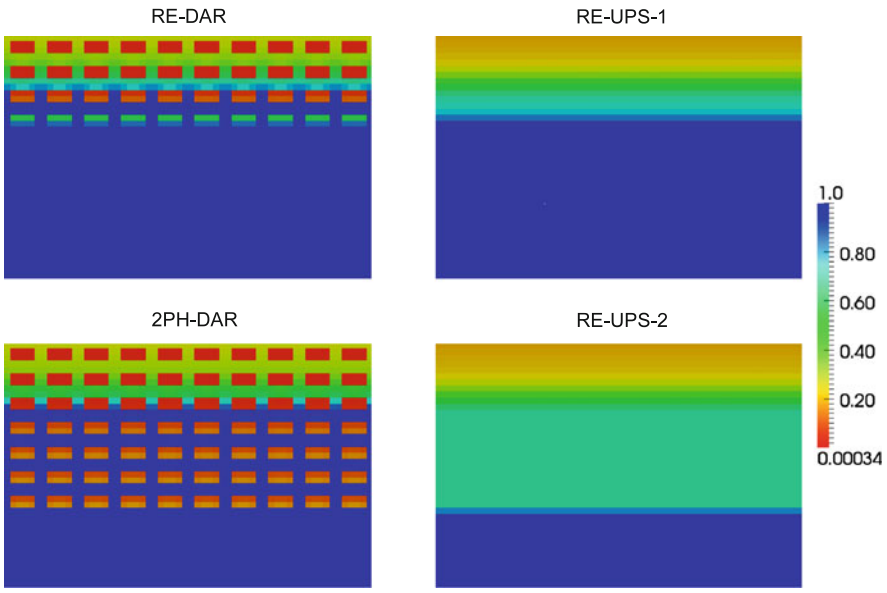


**Fig. 7.9** Example 1: Distribution of the water saturation at $t = 8160\,\mathrm{s}$, notation as in Fig. 7.6

pronounced. According to the 2PH-DAR solution, as the water table is risen the background material in the whole domain becomes fully saturated, before the previously drained inclusions reach full saturation. The blocking of flow paths for air leads to trapping of large quantities of air in the inclusions. The inclusions remain unsaturated till the end of the simulation. In contrast, RE-DAR solution shows that all inclusions become fully saturated at the end of the simulation. While there are some unsaturated inclusions immediately behind the wetting front in the background material, they are quickly filled with water, as can be seen in Fig. 7.9. Thus, the Richards equation predicts a reversible drainage–infiltration process, which is similar to the one observed for homogeneous medium, Fig. 7.5. On the other hand, the two-phase flow model describes a reversible phenomenon only in the case of homogeneous medium, while in the presence of coarse-textured inclusions the initial fully water-saturated state is not recovered.

As can be seen from Fig. 7.6, the upscaled model based on the standard approach, RE-UPS-1, follows very closely the solution of Darcy-scale Richards equation, RE-DAR. This proves the accuracy of the homogenization approach, but both solutions are far from the two-phase solution, which should be considered as the reference point. In contrast, the modified approach, RE-UPS-2, is in a reasonable agreement with the 2PH-DAR model, and correctly captures the irreversibility of the drainage–infiltration cycle. This suggest that the Richards equation can be used to describe unsaturated water flow in porous media showing heterogeneity with respect to the air entry pressure, on condition that the effective functions are appropriately modified.

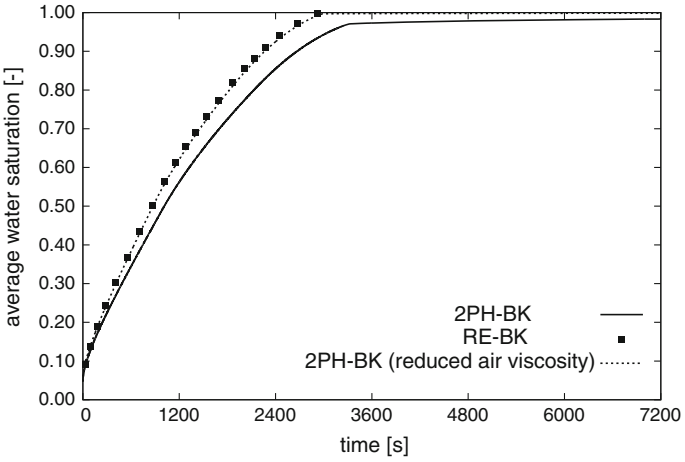


**Fig. 7.10** Example 2: Evolution of the average water saturation in homogeneous domain

### *7.2.3 Example 2: Two-Dimensional Infiltration*

The second example represents two-dimensional downward infiltration in an initially dry porous medium, Fig. 7.2b. The initial value of the water pressure is $p_w = -9810\,\text{Pa}$ (water pressure head of $h_w = -1\,\text{m}$) and the air is at atmospheric pressure $p_a = 0$. At the left part of the top boundary, the water pressure is instantaneously risen to the value $p_w = 0$, while the air pressure is kept at atmospheric value, which implies full water saturation. All other boundary segments are considered impermeable for water and open for the atmospheric air ($p_a = 0$). Since the upscaled problem is also two-dimensional, all numerical simulations were performed on the same grid of 60 by 40 elements.

In contrast to the previous example, some differences between the two-phase model and the Richards model can be noticed even for homogeneous medium. The corresponding values of the average saturation in the background material without inclusions are shown in Fig. 7.10. The Richards equation predicts a slightly faster infiltration rate than the two-phase model, while at the end of the simulation the domain becomes wholly water-saturated according to both approaches. As the boundaries are open for air flow, the discrepancy seems to be caused by the viscous resistance to air flow. In fact, decreasing the air viscosity by two orders of magnitude leads to a perfect matching, as shown in Fig. 7.10.

The evolution of average water saturation in heterogeneous medium is plotted in Fig. 7.11, while Figs. 7.12 and 7.13 show the spatial distribution of the water saturation in the domain for two intermediate times. In Fig. 7.11 it can be seen that the presence of inclusions leads to a much larger discrepancy between the Richards and two-phase solutions in terms of the evolution of the average water saturation. In the first case, the whole domain becomes fully water-saturated at the end of

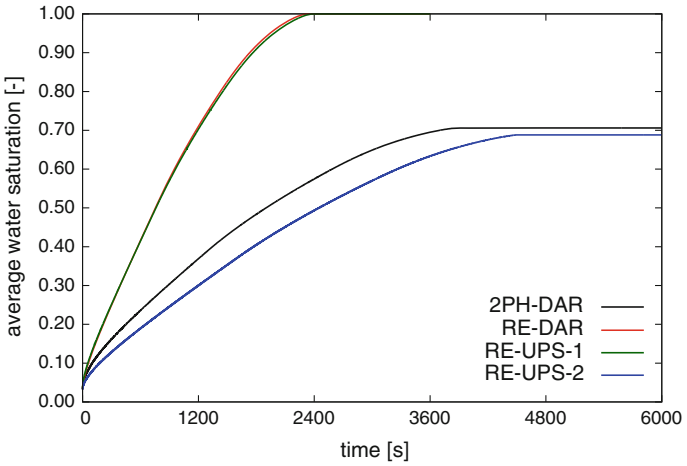


**Fig. 7.11** Example 2: Evolution of the average water saturation in heterogeneous domain, notation as in Fig. 7.6

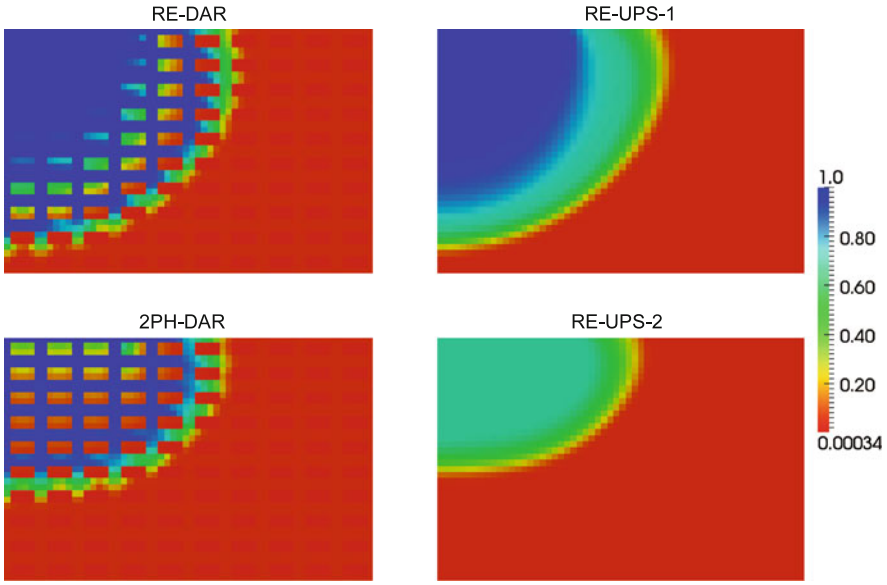


**Fig. 7.12** Example 2: Distribution of the water saturation at $t = 540\,\mathrm{s}$, notation as in Fig. 7.6

the simulation. In the second case, only the background material saturates, while a significant amount of air is trapped in the inclusions. Thus, the final steady-state average saturation is 0.706 according to the two-phase flow model and the infiltration rate represented by the slope of the saturation curve is significantly smaller than in the Richards model.

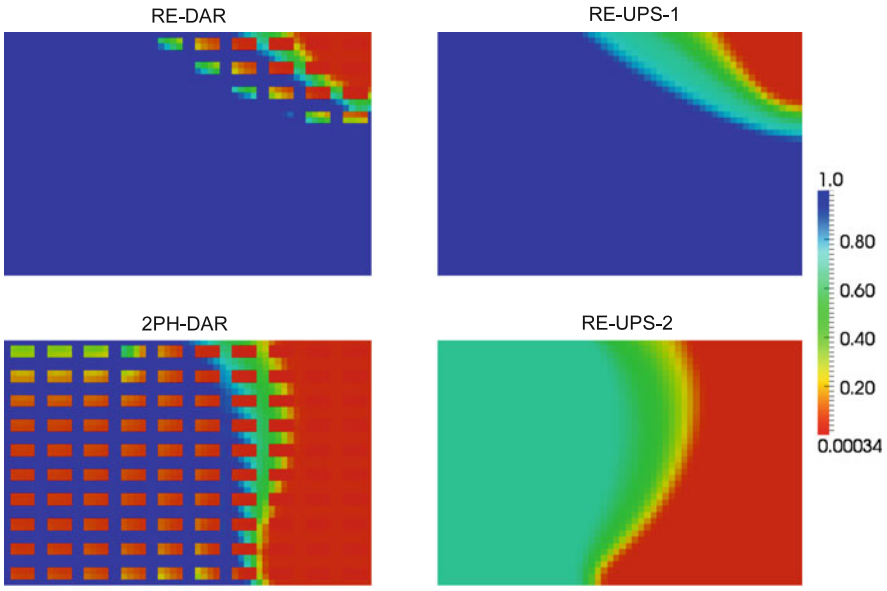


**Fig. 7.13** Example 2: Distribution of the water saturation at $t = 1800$ s, notation as in Fig. 7.6

As far as the upscaled models are considered, one can see that RE-UPS-1 follows the corresponding Darcy-scale solution of the Richards equation (RE-DAR) very closely. In contrast, the difference between the two-phase model and the modified Richards equation RE-UPS-2 is significantly larger than in the previous example, although a qualitative agreement can be observed. While the final steady state saturation of RE-UPS-2 (0.688) is only slightly smaller than the corresponding saturation obtained from 2PH-DAR, more pronounced differences are observed in the infiltration rate, which is lower in the RE-UPS-2 approach. A possible reason for these discrepancies may be a more important role played by gravity and viscous forces, compared to the previous test case. A closer examination of Fig. 7.13 reveals that the saturation in inclusions at the end of simulation is not uniform. In particular, the inclusions close to the infiltration boundary have much higher saturation than the value corresponding to the entry pressure in the background material $S_w = 0.064$. The actual values reach locally 0.578. In the initial stages of the infiltration, the viscous and gravitational forces are important and the capillary equilibrium assumption does not hold for the periodic cells close to the infiltration boundary. Since the water saturation is higher than the one predicted from the capillary equilibrium model, the equivalent permeability of the cell with respect to water is also significantly increased. Consequently, the water infiltration according to 2PH-DAR solution proceeds faster than in the RE-UPS-2 approach, based on the assumption of local capillary equilibrium. Nevertheless, the modified upscaled model RE-UPS-2 is considerably closer to the reference two-phase solution than either the Darcy-scale Richards equation or the upscaled Richards equation without entry pressure effects.

## References


1. Braun C, Helmig R, Manthey S (2005) Macro-scale effective constitutive relationships for two phase flow processes in heterogeneous porous media with emphasis on the relative permeability-saturation relationship. J Contam Hydrol 76(1–2):47–85. doi:10.1016/j.jconhyd.2004.07.009
2. Eichel H, Helmig R, Neuweiler I, Cirpka O (2005) Upscaling of two-phase flow processes in porous media. In: Das D, Hassanizadeh S (ed) Upscaling multiphase flow in porous media, Springer, New York, pp 237–257
3. Jonoud S, Jackson M (2008) New criteria for the validity of steady-state upscaling. Transp Porous Media 71(1):53–73. doi:10.1007/s11242-007-9111-x
4. Mikelic A, van Duijn C, Pop I (2002) Effective equations for two-phase flow with trapping on the micro scale. SIAM J Appl Math 62(5):1531–1568. doi:10.1137/S0036139901385564
5. Quintard M, Whitaker S (1988) Two-phase flow in heterogeneous porous media: The method of large scale averaging. Transp Porous Media 3(4):357–413. doi:10.1007/BF00233177
6. Saez A, Otero C, Rusinek I (1989) The effective homogeneous behavior of heterogeneous porous media. Transp Porous Media 4(3):213–238. doi:10.1007/BF00138037
7. Stephen K, Pickup G, Sorbie K (2001) The local analysis of changing force balances in immiscible incompressible two-phase flow. Transp Porous Media 45(1):63–88. doi:10.1023/A:1011850618324
8. Szymkiewicz A, Helmig R, Kuhnke H (2011) Two-phase flow in heterogeneous porous media with non-wetting phase trapping. Transp Porous Media 86(1):27–47. doi:10.1007/s11242-010-9604-x
9. Szymkiewicz A, Helmig R, Neuweiler I (2012) Upscaling unsaturated flow in binary porous media with air entry pressure effects. Water Resour Res 48:W04522. doi:10.1029/2011WR010893
10. van Duijn C, Eichel H, Helmig R, Pop I (2007) Effective equations for two-phase flow in porous media: the effect of trapping at the micro-scale. Transp Porous Media 69(3):411–428. doi:10.1007/s11242-006-9089-9
11. Vasin M, Lehmann P, Kaestner A, Hassanein R, Nowak W, Helmig R, Neuweiler I (2008) Drainage in heterogeneous sand columns with different geometric structures. Adv Water Resour 31(9):1205–1220. doi:10.1016/j.advwatres.2008.01.004